Biomechanics and Modeling in Mechanobiology manuscript No.
(will be inserted by the editor)

A model for the compressible, viscoelastic behavior of human amnion addressing tissue variability through a single parameter

Arabella Mauri* · **Alexander E. Ehret*** · **Davide S.A. De Focatiis** · **Edoardo Mazza**

Received: date / Accepted: date

Abstract A viscoelastic, compressible model is proposed to rationalize the recently reported response of human amnion in multiaxial relaxation and creep experiments. The theory includes two viscoelastic contributions responsible for the short- and long-term time-dependent response of the material. These two contributions can be related to physical processes: water flow through the tissue and dissipative characteristics of the collagen fibers, respectively. An accurate agreement of the model with the mean tension and kinematic response of amnion in uniaxial relaxation tests was achieved. By variation of a single linear factor that accounts for the variability among tissue samples, the model provides very sound predictions not only of the uniaxial relaxation but also of the uniaxial creep and strip-biaxial relaxation behavior of individual samples. This suggests that a wide range of viscoelastic behaviors due to patient-specific variations in tissue composition can be represented by the model without the need of recalibration and parameter identification.

Keywords Biological Membrane · Compressible Viscoelastic Model · Specimen Variability · Human Amnion · Creep · Stress Relaxation

*AM and AEE share first authorship of this article.

A. Mauri · A. E. Ehret
Institute of Mechanical Systems, Department of Mechanical and Process Engineering, ETH Zurich, 8092 Zurich, Switzerland
Tel.: +41-44-6322630
Fax: +41-44-6321145
E-mail: {mauri,ehret}@imes.mavt.ethz.ch

D. S. A. De Focatiis
Division of Materials, Mechanics and Structures, Faculty of Engineering, University of Nottingham, NG7 2RD Nottingham, United Kingdom

E. Mazza
Institute of Mechanical Systems, Department of Mechanical and Process Engineering, ETH Zurich, 8092 Zurich, Switzerland
Empa. Swiss Federal Laboratories for Materials Science and Technology, 8600 Dübendorf, Switzerland

1 Introduction

The formulation and validation of a suitable constitutive model for the human amnion is important to better predict complex in vivo loading conditions and represents the first step towards the development of numerical simulation methods to address clinically relevant questions conditions as well as to analyze in detail the results of mechanical experiments for the determination of tissue strength and fracture properties. Such a model represents the first step towards the development of numerical simulation tools to address clinical questions, as for example potential structural weakening caused by prenatal surgery [Devlieger et al, 2006; Beck et al, 2012] or increased rupture risk associated with cervical opening or pelvic floor laxity [Menon et al, 2015].

Amnion, the inner of the fetal membranes (FMs), is a thin and strong tissue in contact with the amniotic fluid [Bourne, 1962; Mauri et al, 2013]. In terms of mechanical properties it is considered to be the determining structure [Oxlund et al, 1990; Oyen et al, 2006] that surrounds and protects the fetus during gestation. Recently, a comprehensive experimental campaign has been performed to investigate the time- and history-dependent behavior of the human amnion [Mauri et al, 2015c; Perrini et al, 2015]. The results of these uniaxial and biaxial experiments confirmed the substantial relaxation of the tension at constant strain reported for FM tissues in previous studies [Lavery and Miller, 1977;

Oyen et al, 2004, 2005] along with the limited strain accumulation in creep experiments also observed in other soft tissues [Anssari-Benam et al, 2012; Grashow et al, 2006; Hingorani et al, 2004; Thornton et al, 2001]. New microscopic insight [Mauri et al, 2015b] revealed substantial thickness changes in uniaxial and biaxial extension which, together with the large lateral contraction observed in uniaxial loading [Bürzle and Mazza, 2013; Mauri et al, 2015c], imply that the human amnion is able to considerably change its volume by changing its water content. Based on a combination of macro- and microscopic results, it was hypothesized in Mauri et al [2015c] that the relaxation behavior can be separated into a short-term phase, during which the tissue volume is reduced, water is expelled and fibers reorient, and a long-term phase, which is characterized by the dissipative, time-dependent behavior of the fibers themselves.

Accordingly, a suitable modeling framework is required in order to capture these compressible and time-dependent characteristics. Only very few contributions have concerned themselves with models of the time-dependent behavior of FM tissue. A quasi-linear viscoelastic model was considered and found inadequate for amnion by Oyen et al [2005]. Prévost [2006] suggested a formulation based on a multiplicative decomposition of the in-plane deformation gradient into elastic and viscous parts, which was, however, not further studied or compared to experimental data. In general, a large number of viscoelastic theories have been proposed or customized for various soft tissues [see e.g. Ehret, 2011], including the mentioned quasilinear [see Fung, 1993] and fractional order viscoelastic models [e.g. Doehring et al, 2005], explicitly rate-dependent theories [e.g. Limbert and Middleton, 2004] or models with tensor or scalar valued strain- or stress-like internal variables [e.g. Holzapfel, 1996; Nguyen et al, 2007; Ehret and Itskov, 2009]. Time-dependent behavior is also intrinsic to fluid-saturated porous media, and the according multiphasic theory has been used to rationalize the mechanics of soft tissues such as tendon, cartilage or intervertebral disc tissues [Ateshian et al, 2004; Atkinson et al, 1997; Ehlers et al, 2006; Jacobs et al, 2014].

The soft tissue model proposed by Rubin and Bodner [2002] provides a versatile framework [Helfenstein et al, 2010] to represent the mechanical behavior of collagenous tissues [Mazza et al, 2005; Barbarino et al, 2011; Bürzle and Mazza, 2013; Weickenmeier and Jabareen, 2014; Flynn and Rubin, 2014; Safadi and Rubin, 2014] offering the possibility to include dissipative, inelastic characteristics. In application to FM tissues, Jabareen et al [2009] used an elastic isotropic formulation of the Rubin-Bodner (RB) model to represent the uniaxial response of the amnion. An orthotropic extension with representative fiber families distributed within the membrane plane was proposed by Bürzle and Mazza [2013] to capture the response of amnion under uniaxial and biaxial loads [Bürzle et al, 2013], and the extremely large transverse contraction in uniaxial tension tests [Bürzle and Mazza, 2013]. In the present contribution, a compressible, time-dependent formulation of the RB model is used to rationalize the time dependent behavior of the amnion. The model is calibrated from uniaxial relaxation experiments and validated by comparison with strip-biaxial relaxation as well as uni- and equibiaxial creep tests [Mauri et al, 2015c].

Human biological tissues are characterized by large intra- and inter-subject variability [e.g. Bürzle et al, 2013; Pierce et al, 2015], and representative mean curves of the tissue are usually obtained by testing of, and averaging over a large number of specimens. This variability in human tissues is not an experimental artifact, but rather an intrinsic and integral property of the material, viz. the healthy human tissue. Material parameters describing the mechanical characteristics of soft tissues such as FM [Jabareen et al, 2009; Bürzle et al, 2013], aorta [Schriefl et al, 2015; Reeps et al, 2013] and liver tissue [Mazza et al, 2007; Yarpuzlu et al, 2014] have been correlated with histological or biochemical properties to understand effects arising from tissue heterogeneity. In the present contribution, we propose a straightforward modeling approach that includes the characteristic human variability arising from the differences in tissue by a single scalar "patient- or region-specific" parameter, and a set of general "tissue-specific" parameters that holds for all tested samples from different membranes.

2 Constitutive Model

2.1 Kinematic framework

Let $\mathbf{F} = \mathrm{Grad}\,\boldsymbol{\chi}(\boldsymbol{X}, t)$ denote the deformation gradient of the motion $\boldsymbol{\chi}(\boldsymbol{X}, t)$ of a particle with position $\boldsymbol{X}$ of a material body in the reference state at time $t = t_0$. Here and henceforth, the dependence of kinematic quantities on space and time will not be explicitly indicated unless needed to distinguish between different events in time. The volume change of infinitesimal volume elements at $(\boldsymbol{X}, t)$ is expressed by $J = \det \mathbf{F}$, $\mathbf{l} = \dot{\mathbf{F}}\mathbf{F}^{-1}$ denotes the spacial velocity gradient $\mathbf{d} = (\mathbf{l} + \mathbf{l}^{\mathrm{T}})/2$ is the symmetric rate of deformation tensor and the left Cauchy-Green tensor reads $\mathbf{b} = \mathbf{F}\mathbf{F}^{\mathrm{T}}$. The collagen structure in the tissue is represented by N representative families of fibers whose axes are aligned with the unit vectors $\boldsymbol{M}^i$,

$i = 1, 2, ..., N$, in the reference state. An affine transformation maps them onto the set of non-unit vectors $\boldsymbol{m}^i = \mathbf{F}\boldsymbol{M}^i$ with length $\lambda_{f,i} = |\boldsymbol{m}^i|$. Note that collagen fibers are not expected to deform affinely with the extracellular matrix; thus the families of fibers introduced in these models represent the collagen network in a phenomenological sense. The temporal change of $\mathbf{b}$ and the vectors $\boldsymbol{m}^i$ is given by the material time derivatives [cf. e.g. Rubin, 1996; Rubin and Bodner, 2002; Haupt, 2002]

$$\dot{\mathbf{b}} = \mathbf{l}\mathbf{b} + \mathbf{b}\mathbf{l}^{\mathrm{T}}, \quad \dot{\boldsymbol{m}}^i = \mathbf{l}\boldsymbol{m}^i, \;\; i = 1, 2, .., N. \tag{1}$$

Due to dissipative mechanisms, the strains associated with storage of elastic energy in the matrix and fibers, expressed by $\mathbf{b}_{\mathrm{e}}$ and $\boldsymbol{m}_{\mathrm{e}}^i$, respectively, may differ from the total deformations. In line with the theory outlined in [Rubin, 1994a,b, 1996; Rubin and Bodner, 2002] the material rates of the kinematic quantities relating to these elastic deformations are expressed in a general form by

$$\begin{aligned} &\dot{\mathbf{b}}_{\mathrm{e}} = \mathbf{l}\mathbf{b}_{\mathrm{e}} + \mathbf{b}_{\mathrm{e}}\mathbf{l}^{\mathrm{T}} - \mathbf{a}, \\ &\dot{\boldsymbol{m}}_{\mathrm{e}}^i = \mathbf{l}\boldsymbol{m}_{\mathrm{e}}^i - \boldsymbol{a}^i, \; i = 1, 2, ..., N, \end{aligned} \tag{2}$$

where the tensor $\mathbf{a}$ and vectors $\boldsymbol{a}^i$ specify the rates of the inelastic deformations [cf. Rubin and Bodner, 2002]. Integration of the rate equations (2) finally defines the history of b_e and m_e^i over time. The terms a and a_i can be specified in order to incorporate a specific viscoelastic behavior. While in the original model as well as recent extensions [Rubin and Bodner, 2002; Weickenmeier and Jabareen, 2014] it was assumed that dissipation occurs due to viscoplastic *isochoric* deformations of the isotropic *matrix* material, the model presented herein takes into account dissipative mechanisms arising from viscoelasticity associated with the *volumetric* deformation of the *matrix* and the deformation of the *fibers*. This is in agreement with the observations in our recent study [Mauri et al, 2015c] that the temporal decay of tension in relaxation tests can be separated into a short and a long-term phase, which were attributed to tissue volume reduction and dissipative fiber behavior, respectively.

2.2 Dissipative volumetric and fiber deformations

Applying the multiplicative decomposition of the deformation gradient $\mathbf{F} = J^{1/3}\bar{\mathbf{F}}$ [Flory, 1961] into volumetric and volume preserving parts, the material time derivative of the left Cauchy-Green tensor $(1)_1$ has the decoupled form

$$\dot{\mathbf{b}} = \mathbf{l}\mathbf{b} + \mathbf{b}\mathbf{l}^{\mathrm{T}} = \dot{\overline{J^{2/3}\bar{\mathbf{b}}}} = \frac{2}{3}J^{-1/3}\dot{J}\bar{\mathbf{b}} + J^{2/3}\dot{\bar{\mathbf{b}}}. \tag{3}$$

The two material time derivatives in (3) calculate as

$$\dot{J} = \frac{J}{2}\mathbf{b}^{-1} : \dot{\mathbf{b}} = J\,\mathrm{tr}\mathbf{d}, \quad \dot{\bar{\mathbf{b}}} = \mathbf{l}\bar{\mathbf{b}} + \bar{\mathbf{b}}\mathbf{l}^{\mathrm{T}} - \frac{2}{3}(\mathrm{tr}\mathbf{d})\bar{\mathbf{b}}, \tag{4}$$

where the second one $(4)_2$ ensures that $\bar{\mathbf{b}}$ remains unimodular during the evolution [Rubin, 1994a]. Eqns. ((3) and (4)) suggest that dissipation associated with volumetric and isochoric deformations can be considered separately. As stated in the previous section, we attribute the dissipation in the matrix exclusively to volumetric changes. This assumption implies that the material rate of the isochoric elastic left Cauchy-Green tensor remains unaltered from $(4)_2$ so that

$$\dot{\bar{b}}_e = \dot{\bar{b}}. \tag{5}$$

Since we assume the dissipation in the matrix to be related to the volumetric changes only, the material rate of the deviatoric elastic left Cauchy-Green tensor remains unaltered from (3) so that $\dot{\bar{\mathbf{b}}}_{\mathrm{e}} = \dot{\bar{\mathbf{b}}}$. The rate of elastic volume change $J_{\mathrm{e}} = \sqrt{\det \mathbf{b}_{\mathrm{e}}}$, however, is prescribed by

$$\dot{J}_{\mathrm{e}} = J_{\mathrm{e}}\,\mathrm{tr}\mathbf{d} - \Gamma_{\mathrm{M}} \tag{6}$$

and differs from $\dot{J}$ by the rate of dissipative volume change Γ_{M}, which is generally a function of all kinematic variables. Reinserting (6) into (3) and replacing $\mathbf{b}_{\mathrm{e}}$ for $\mathbf{b}$ and J_{e} for J, one obtains

$$\begin{aligned} \dot{\mathbf{b}}_{\mathrm{e}} &= \frac{2}{3}J_{\mathrm{e}}^{2/3}(\mathrm{tr}\mathbf{d})\bar{\mathbf{b}}_{\mathrm{e}} + J_{\mathrm{e}}^{2/3}\left(\mathbf{l}\bar{\mathbf{b}}_{\mathrm{e}} + \bar{\mathbf{b}}_{\mathrm{e}}\mathbf{l}^{\mathrm{T}} - \frac{2}{3}(\mathrm{tr}\mathbf{d})\bar{\mathbf{b}}_{\mathrm{e}}\right) \\ &\quad - \frac{2}{3}J_{\mathrm{e}}^{-1/3}\Gamma_{\mathrm{M}}\bar{\mathbf{b}}_{\mathrm{e}} = \mathbf{l}\mathbf{b}_{\mathrm{e}} + \mathbf{b}_{\mathrm{e}}\mathbf{l}^{\mathrm{T}} - \frac{2}{3}J_{\mathrm{e}}^{-1}\Gamma_{\mathrm{M}}\mathbf{b}_{\mathrm{e}}, \end{aligned} \tag{7}$$

hence specifying the tensor $\mathbf{a}$ in $(2)_1$ as

$$\mathbf{a} = \frac{2}{3}J_{\mathrm{e}}^{-1}\Gamma_{\mathrm{M}}\mathbf{b}_{\mathrm{e}}. \tag{8}$$

The evolution law for the elastic component of the fiber vectors $(2)_2$ is subject to the requirement of invariance under superimposed rigid body motions [Rubin, 1994a]. A pull-back of the vector $\boldsymbol{m}_{\mathrm{e}}$ to the reference configuration (the index i is omitted for the sake of brevity) yields $\boldsymbol{M}_{\mathrm{e}} = \mathbf{F}^{-1}\boldsymbol{m}_{\mathrm{e}}$ with material time derivative

$$\dot{\boldsymbol{M}}_{\mathrm{e}} = \dot{\overline{\mathbf{F}^{-1}\boldsymbol{m}_{\mathrm{e}}}} = \mathbf{F}^{-1}\dot{\boldsymbol{m}}_{\mathrm{e}} - \mathbf{F}^{-1}\mathbf{l}\boldsymbol{m}_{\mathrm{e}}. \tag{9}$$

The Lie time derivative, see [Holzapfel, 2000, Sec. 2.8, 5.3], $\dot{\boldsymbol{m}}_{\mathrm{e}} - \mathbf{l}\boldsymbol{m}_{\mathrm{e}} = \mathbf{F}(\dot{\overline{\mathbf{F}^{-1}\boldsymbol{m}_{\mathrm{e}}}})$ is objective since for an arbitrary orthogonal transformation $\mathbf{Q} = \mathbf{Q}(t)$ superimposed onto the current state of deformation, so that $\mathbf{F}^* = \mathbf{Q}\mathbf{F}$ and $\boldsymbol{m}_{\mathrm{e}}^* = \mathbf{Q}\boldsymbol{m}_{\mathrm{e}}$, one verifies

$$\mathbf{F}^*(\dot{\overline{\mathbf{F}^{*-1}\boldsymbol{m}_{\mathrm{e}}^*}}) = \mathbf{F}^*\dot{\boldsymbol{M}}_{\mathrm{e}} = \mathbf{Q}\,(\dot{\boldsymbol{m}}_{\mathrm{e}} - \mathbf{l}\boldsymbol{m}_{\mathrm{e}}) \tag{10}$$

and, accordingly, invariance of the evolution equation $(2)_2$ imposes that $\boldsymbol{a}$ likewise transforms as[1] $\boldsymbol{a}^* = \mathbf{Q}\boldsymbol{a}$. In the following, the particular representations

$$\boldsymbol{a}^i = \Gamma_{\mathrm{F}}^i \boldsymbol{m}_{\mathrm{e}}^i \tag{11}$$

are considered with scalar, objective functions Γ_{F}^i of the kinematic variables $\mathbf{b}$, $\mathbf{b}_{\mathrm{e}}$ and all $\boldsymbol{m}_{\mathrm{e}}^k$, $k = 1, 2, ..., N$.

2.3 Constitutive assumptions

Although generally inappropriate to depict the complexity of the non-linear dissipative model, the image of a rheological scheme with springs and dashpots facilitates understanding the constitutive assumptions. Fibers can be imagined as parallel viscoelastic "Maxwell-type" elements. Strain-energy storage is only related to the length λ_{e} of the fiber vectors $\boldsymbol{m}_{\mathrm{e}}$. The matrix is represented by two further, parallel components: a spring depending on the total deformations ($\mathbf{b}$) and a "Maxwell-type" element, whose elastic part experiences the deformations $\mathbf{b}_{\mathrm{e}}$. Restricting to a reduced set of invariants [see e.g. Ehret and Itskov, 2007], this implies a free energy function of the form

$$\Psi = \hat{\Psi}(I, J, I_{\mathrm{e}}, J_{\mathrm{e}}, \lambda_{\mathrm{e},1}, ..., \lambda_{\mathrm{e},N}), \tag{12}$$

where Ψ is the free strain energy per unit reference volume and the scalar arguments are given by

$$I = \mathrm{tr}\mathbf{b},\ J = \sqrt{\det \mathbf{b}}, \quad I_{\mathrm{e}} = \mathrm{tr}\mathbf{b}_{\mathrm{e}},\ J_{\mathrm{e}} = \sqrt{\det \mathbf{b}_{\mathrm{e}}},$$
$$\lambda_{\mathrm{e},i} = |\boldsymbol{m}|_{\mathrm{e},i},\ i = 1, 2, ..., N. \tag{13}$$

The material time derivative of Eqn. (12) yields in view of Eqns. ((2), (7) and (11)),

$$\begin{aligned}
\dot{\Psi} &= \frac{\partial \Psi}{\partial I}\dot{I} + \frac{\partial \Psi}{\partial J}\dot{J} + \frac{\partial \Psi}{\partial I_{\mathrm{e}}}\dot{I}_{\mathrm{e}} + \frac{\partial \Psi}{\partial J_{\mathrm{e}}}\dot{J}_{\mathrm{e}} + \sum_{i=1}^{N}\frac{\partial \Psi}{\partial \lambda_{\mathrm{e},i}}\dot{\lambda}_{\mathrm{e},i} \\
&= \frac{\partial \Psi}{\partial I}\mathbf{I} : \dot{\mathbf{b}} + \frac{\partial \Psi}{\partial J}\frac{J}{2}\mathbf{b}^{-1} : \dot{\mathbf{b}} + \frac{\partial \Psi}{\partial I_{\mathrm{e}}}\mathbf{I} : \dot{\mathbf{b}}_{\mathrm{e}} \\
&\quad + \frac{\partial \Psi}{\partial J_{\mathrm{e}}}\frac{J_{\mathrm{e}}}{2}\mathbf{b}_{\mathrm{e}}^{-1} : \dot{\mathbf{b}}_{\mathrm{e}} + \sum_{i=1}^{N}\frac{\partial \Psi}{\partial \lambda_{\mathrm{e},i}}\lambda_{\mathrm{e},i}^{-1}\,\boldsymbol{m}_{\mathrm{e}}^i \cdot \dot{\boldsymbol{m}}_{\mathrm{e}}^i \\
&= \left[2\frac{\partial \Psi}{\partial I}\mathbf{b} + 2\frac{\partial \Psi}{\partial I_{\mathrm{e}}}\mathbf{b}_{\mathrm{e}} + \left(\frac{\partial \Psi}{\partial J}J + \frac{\partial \Psi}{\partial J_{\mathrm{e}}}J_{\mathrm{e}}\right)\mathbf{I} \right. \\
&\qquad \left. + \sum_{i=1}^{N}\frac{\partial \Psi}{\partial \lambda_{\mathrm{e},i}}\lambda_{\mathrm{e},i}^{-1}\boldsymbol{m}_{\mathrm{e}}^i \otimes \boldsymbol{m}_{\mathrm{e}}^i\right] : \mathbf{d} \\
&\quad - J_{\mathrm{e}}^{-1}\Gamma_{\mathrm{M}}\frac{1}{3}\left(2\frac{\partial \Psi}{\partial I_{\mathrm{e}}}\mathbf{b}_{\mathrm{e}} + \frac{\partial \Psi}{\partial J_{\mathrm{e}}}J_{\mathrm{e}}\mathbf{I}\right) : \mathbf{I} \\
&\quad - \sum_{i=1}^{N}\lambda_{\mathrm{e},i}\frac{\partial \Psi}{\partial \lambda_{\mathrm{e},i}}\,\Gamma_{\mathrm{F}}^i.
\end{aligned} \tag{14}$$

For convenience, we separate the Cauchy stress $\boldsymbol{\sigma}$ in matrix ($\boldsymbol{\sigma}_{\mathrm{M}}, \boldsymbol{\sigma}_{\mathrm{Me}}$) and fiber ($\boldsymbol{\sigma}_{\mathrm{Fe}}$) parts. The Clausius-Planck form of the second law of thermodynamics [see e.g. Holzapfel, 2000], can hence be written as

$$J\boldsymbol{\sigma} : \mathbf{d} - \dot{\Psi} = J(\boldsymbol{\sigma}_{\mathrm{M}} + \boldsymbol{\sigma}_{\mathrm{Me}} + \boldsymbol{\sigma}_{\mathrm{Fe}}) : \mathbf{d} - \dot{\Psi} \geq 0, \tag{15}$$

and inserting Eqn. (14), one identifies the stress contributions

$$\begin{aligned}
\boldsymbol{\sigma}_{\mathrm{M}} &= \frac{2}{J}\frac{\partial \Psi}{\partial I}\mathbf{b} + \frac{\partial \Psi}{\partial J}\mathbf{I}, \\
\boldsymbol{\sigma}_{\mathrm{Me}} &= \frac{2}{J}\frac{\partial \Psi}{\partial I_{\mathrm{e}}}\mathbf{b}_{\mathrm{e}} + \frac{J_{\mathrm{e}}}{J}\frac{\partial \Psi}{\partial J_{\mathrm{e}}}\mathbf{I}, \\
\boldsymbol{\sigma}_{\mathrm{Fe}} &= \frac{1}{J}\sum_{i=1}^{N}\frac{\partial \Psi}{\partial \lambda_{\mathrm{e},i}}\frac{1}{\lambda_{\mathrm{e},i}}\boldsymbol{m}_{\mathrm{e}}^i \otimes \boldsymbol{m}_{\mathrm{e}}^i.
\end{aligned} \tag{16}$$

The remaining part imposes the thermodynamic restriction

$$J_{\mathrm{e}}^{-1}\Gamma_{\mathrm{M}}\frac{1}{3}J\boldsymbol{\sigma}_{\mathrm{Me}} : \mathbf{I} + \sum_{i=1}^{N}\lambda_{\mathrm{e},i}\frac{\partial \Psi}{\partial \lambda_{\mathrm{e},i}}\,\Gamma_{\mathrm{F}}^i \geq 0 \tag{17}$$

that guarantees a non-negative rate of local entropy production [see e.g. Coleman and Gurtin, 1967; Holzapfel, 2000].

2.4 Particular forms of the constitutive equations

Starting from the FM model by Bürzle and Mazza [2013], we apply three major modifications: the matrix material is assumed to be compressible and viscoelastic, and the representative set of fibers, which was originally equally spaced within the membrane plane, is given a small alternating off-plane inclination $\pm\vartheta$. The unit vectors, defining the directions of the N representative fibers, thus read (Remark 1)

$$\begin{aligned}
\boldsymbol{M}_i &= \cos\phi_i \sin\theta \boldsymbol{e}_1 + \sin\phi_i \sin\theta \boldsymbol{e}_2 + (-1)^i \cos\theta \boldsymbol{e}_3, \\
\phi_i &= \frac{\pi}{N}\left(i - \frac{3}{2}\right), \quad \theta = \frac{\pi}{2} - \vartheta.
\end{aligned} \tag{18}$$

Moreover, the free energy representation (12) is specified so that the viscoelastic matrix contribution depends only on the volume change J_{e}, i.e. it becomes independent of I_{e}. This reflects the assumption that J_{e} represents the volume change due to compression of the fluid contained in the matrix, which is small due to the very low compressibility of water. The free energy for the so-obtained variant of the RB model reads [cf. Rubin and Bodner, 2002; Bürzle and Mazza, 2013]

$$\Psi = \frac{\mu_0}{2q}(e^{qg} - 1), \quad g = g_1 + g_2 + g_3. \tag{19}$$

[1] In Rubin's work [Rubin, 1994a,b, 1996] this is satisfied by dissipative rates of the form $\boldsymbol{a} = \mathbf{L}_{\mathrm{p}}\boldsymbol{m}_{\mathrm{e}}$, where the second-order tensor $\mathbf{L}_{\mathrm{p}}$ transforms as $\mathbf{L}_{\mathrm{p}}^* = \mathbf{Q}\mathbf{L}_{\mathrm{p}}\mathbf{Q}^{\mathrm{T}}$ under superposed rigid body motions. The approach in Eq. (11) is consistent with the particular choice $\mathbf{L}_{\mathrm{p}} = \Gamma_{\mathrm{F}}\mathbf{I}$.

Compared to the original RB model [Rubin and Bodner, 2002], the volumetric term g_1 depends on the viscoelastic volumetric deformations J_e and is given by a penalty function for nearly-incompressible hyperelastic materials [Simo and Taylor, 1982], in agreement with the just mentioned weak compressibility of water. Moreover, g_2 represents the contribution of the compressible solid matrix and is hence given in terms of the compressible neo-Hookean model [see e.g. Holzapfel, 2000]. Finally, the affine fiber stretches in the fiber strain-energy were replaced by λ_e^i and the parameter $\bar{m}_3 = N\, m_3$ was introduced in order to make the material law "independent" of the number of fiber families used to establish a quasi-isotropic in-plane response. Hence g_1, g_2, g_3 read

$$
\begin{aligned}
g_1 &= g_1(J_\mathrm{e}) = m_1 \left[(J_\mathrm{e}-1)^2 + (\ln J_\mathrm{e})^2\right], \\
g_2 &= g_2(I,J) = m_2\,(I-3) + \frac{m_2}{m_5}\left(J^{-2m_5}-1\right), \\
g_3 &= g_3(\lambda_{\mathrm{e},i}) = \frac{\bar{m}_3}{m_4}\frac{1}{N}\sum_{i=1}^{N}\left\langle \lambda_{\mathrm{e},i}-1\right\rangle^{2m_4},
\end{aligned}
\tag{20}
$$

where $\langle\bullet\rangle$ denote Macaulay brackets. In view of (16), the Cauchy stress tensor $\boldsymbol{\sigma} = \boldsymbol{\sigma}_\mathrm{Me} + \boldsymbol{\sigma}_\mathrm{M} + \boldsymbol{\sigma}_\mathrm{Fe}$ is thus given by

$$
\begin{aligned}
\boldsymbol{\sigma}_\mathrm{Me} &= \frac{\mu_0 e^{qg}}{J} m_1 \left(J_\mathrm{e}^2 - J_\mathrm{e} + \ln J_\mathrm{e}\right)\mathbf{I}, \\
\boldsymbol{\sigma}_\mathrm{M} &= \frac{\mu_0 e^{qg}}{J} m_2 \left(\mathbf{b} - J^{-2m_5}\mathbf{I}\right), \\
\boldsymbol{\sigma}_\mathrm{Fe}^i &= \frac{\mu_0 e^{qg}}{J}\frac{\bar{m}_3}{\lambda_{\mathrm{e},i}}\left\langle \lambda_{\mathrm{e},i}-1\right\rangle^{2m_4-1} \boldsymbol{m}_\mathrm{e}^i \otimes \boldsymbol{m}_\mathrm{e}^i, \\
\boldsymbol{\sigma}_\mathrm{Fe} &= \frac{1}{N}\sum_{i=1}^{N}\boldsymbol{\sigma}_\mathrm{Fe}^i.
\end{aligned}
\tag{21}
$$

Finally, the dissipative rates $\mathit{\Gamma}_\mathrm{M}$ and $\mathit{\Gamma}_\mathrm{F}^i$ have to be defined such that (17) is satisfied. Here, we suggest the simple representations

$$
\begin{aligned}
\mathit{\Gamma}_\mathrm{M} &= k_\mathrm{M} J^{\alpha_\mathrm{M}} \mathrm{tr}(\boldsymbol{\sigma}_\mathrm{Me}), \\
\mathit{\Gamma}_\mathrm{F}^i &= k_\mathrm{F}\lambda_{\mathrm{e},i}\frac{\partial \Psi}{\partial \lambda_{\mathrm{e},i}} = k_\mathrm{F}\mathrm{tr}(J\boldsymbol{\sigma}_\mathrm{Fe}^i)
\end{aligned}
\tag{22}
$$

with three positive constants k_M, k_F and α_M, and chosen such that both the observed uniaxial relaxation and creep responses could be captured. While the second of these equations represents a simple linear relation between the fiber Kirchhoff stress and the inelastic rates $\mathit{\Gamma}_\mathrm{F}^i$, the first one entails a power-law relationship between the volume change of the tissue and the dissipative rate $\mathit{\Gamma}_\mathrm{M}$, which can be motivated by drawing parallels with the fluid flow in porous media (see the discussion Sec. 4.3).

Remark 1 *The alternating off-plane inclination of the fibers in* (18) *does not affect the in-plane quasi-isotropy obtained with N families [cf. Bürzle and Mazza, 2013]. However, it induces a slight asymmetry of the structure with respect to the membrane plane. This is irrelevant if there is no shear across the thickness, as usually assumed for thin membranes. In the general case, this asymmetry can be avoided by tilting the fiber families symmetrically in both directions, i.e.* $+\vartheta$ *and* $-\vartheta$*, thereby doubling their number.*

2.5 Special case: compressible elastic formulation

The constitutive model established by the Eqns. ((18)-(21)) contains as a special case an elastic compressible model suitable to account for the quasi-static behavior of the amnion. This model applies if the time-scale of observation is long enough that the outflow of water has entirely ceased ($J_\mathrm{e} \to 1$) yet short enough that no substantial creep occurs in the fibers ($\lambda_{\mathrm{e},i} \to \lambda_{f,i}$). With these assumptions, it follows from Eqns. (20) and (21) that

$$
\begin{aligned}
g = {} & m_2\,(I-3) + \frac{m_2}{m_5}\left(J^{-2m_5}-1\right) \\
& + \frac{\bar{m}_3}{m_4}\frac{1}{N}\sum_{i=1}^{N}\left\langle \lambda_{f,i}-1\right\rangle^{2m_4},
\end{aligned}
\tag{23}
$$

$$
\begin{aligned}
\boldsymbol{\sigma} = \frac{\mu_0 e^{qg}}{J}\Bigg[& m_2\left(\mathbf{b} - J^{-2m_5}\mathbf{I}\right) \\
& + \frac{1}{N}\sum_{i=1}^{N}\frac{\bar{m}_3}{\lambda_{f,i}}\left\langle \lambda_{f,i}-1\right\rangle^{2m_4-1}(\mathbf{F}\boldsymbol{M}_i)\otimes(\mathbf{F}\boldsymbol{M}_i)\Bigg].
\end{aligned}
\tag{24}
$$

Multiplication of (24) by the current thickness of the membrane yields a refined representation of the model by Bürzle and Mazza [2013, Eq. 10 therein]. Similar to the latter, the refined model yields accurate agreement with the tension and lateral stretch responses in uniaxial tension and provides an excellent prediction of the equibiaxial tension response [Mauri et al, 2015a]. However, while the original, incompressible model implies an increase in thickness in uniaxial tension, the refined model agrees well with the reduction in thickness observed by multiphoton microscopy [Mauri et al, 2015c] as illustrated in Fig. 1.

2.6 Numerical framework

The material model developed in Sec. 2 was implemented in MATLAB (R2013a, The MathWorks, Inc.)

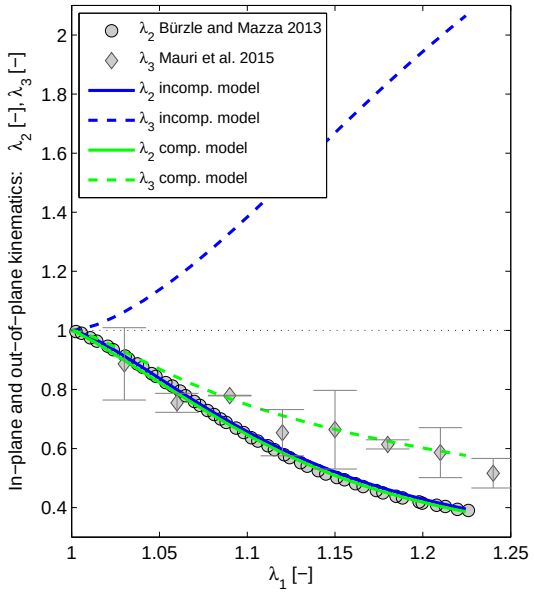

Fig. 1 Comparison of lateral in-plane (λ_2) and out-of-plane (λ_3) stretches vs. stretch in loading direction in uniaxial tension for the incompressible model with planar fibers [Bürzle and Mazza, 2013] and the refined, compressible model with slightly inclined fibers together with corresponding experimental data reported in [Bürzle and Mazza, 2013; Mauri et al, 2015b]. Parameters of the compressible model: $\bar{\mu}_0 = 0.131$ N/mm; $q = 2.96$; $\vartheta = 9.51°$; $m_2 = 0.00228$; $\bar{m}_3 = 41.1$; $m_4 = 1.27$; $m_5 = 0.463$.

to compute the special cases of homogeneous uniaxial, strip- and equi-biaxial tension under time-dependent loading, which necessitated appropriate algorithms to compute the rate equations (2). Procedures to integrate the evolution equations appearing in RB type models have been developed in [Rubin, 1989, 1996; Rubin and Bodner, 2002], and recently by Rubin and Papes [2011] and Hollenstein et al [2013]. The numerical integration of the evolution equations (7) and (11) for $\boldsymbol{m}_\mathrm{e}$ and $\mathbf{b}_\mathrm{e}$ follows the predictor-corrector scheme used to compute the deviatoric elastic left Cauchy-Green tensor in [Rubin and Bodner, 2002, Appendix A]. The recent modifications to obtain the exact result in the case of zero dissipation [Rubin and Papes, 2011; Hollenstein et al, 2013; Flynn and Rubin, 2014], which adopt the idea of a relative deformation gradient from the configurations at time t^n to t^{n+1} [see Simo, 1992; Simo and Hughes, 2000], have been included.

Taking into account that the deformation gradient $\mathbf{F} = \mathbf{F}(\boldsymbol{X}, t^{n+1})$ calculates from the previously achieved value $\mathbf{F}^n = \mathbf{F}(\boldsymbol{X}, t^n)$ as $\mathbf{F} = \mathbf{F}^n + \Delta\mathbf{F}$, an elastic predictor can be calculated, assuming that the whole deformation increment $\Delta\mathbf{F}$ is elastic. To this end, the incremental deformation gradient $\mathbf{h} = \mathbf{F}(\mathbf{F}^n)^{-1}$ is introduced and it is predicted that $\mathbf{F}_\mathrm{e}^* = \mathbf{h}\mathbf{F}_\mathrm{e}^n$. With this, the estimator for $\mathbf{b}_\mathrm{e}$ at $n+1$ reads [cf. Rubin and Papes, 2011; Hollenstein et al, 2013; Flynn and Rubin, 2014]

$$\mathbf{b}_\mathrm{e}^* = \mathbf{h}\mathbf{b}_\mathrm{e}^n\mathbf{h}^\mathrm{T}, \tag{25}$$

independent of the size of the time step Δt. By means of numerical integration of the evolution equation (7), here by the backward Euler method (Remark 3), the predictor can be corrected as

$$\mathbf{b}_\mathrm{e} = \mathbf{b}_\mathrm{e}^* - \Delta t\,\frac{2}{3}J_\mathrm{e}^{-1}\Gamma_\mathrm{M}\,\mathbf{b}_\mathrm{e}, \tag{26}$$

which implies

$$\mathbf{b}_\mathrm{e} = \left[1 + \frac{2\Delta t}{3J_\mathrm{e}}\Gamma_\mathrm{M}\right]^{-1}\mathbf{b}_\mathrm{e}^* = \kappa\mathbf{b}_\mathrm{e}^*, \tag{27}$$

$$J_\mathrm{e} = \sqrt{\det\mathbf{b}_\mathrm{e}} = \kappa^{3/2}\sqrt{\det\mathbf{b}_\mathrm{e}^*} = J_\mathrm{e}^n\kappa^{3/2}\det\mathbf{h} \tag{28}$$

and yields the implicit equation for κ as

$$1 - \left[1 + \frac{2}{3}\frac{\Delta t}{\kappa^{3/2}J_\mathrm{e}^n\,\det\mathbf{h}}\Gamma_\mathrm{M}\right]\kappa = 0. \tag{29}$$

to be solved similar as in [Rubin and Bodner, 2002].

An analogous strategy is suggested to compute the evolving fiber vectors $\boldsymbol{m}_\mathrm{e}^i$. For the sake of clarity, the fiber index i is omitted in what follows, but the same procedure applies to all families of fibers. The elastic predictor is chosen as

$$\boldsymbol{m}_\mathrm{e}^* = \mathbf{h}\,\boldsymbol{m}_\mathrm{e}^n \tag{30}$$

and, in regard of (11), the inelastic correction leads to

$$\begin{aligned}&\boldsymbol{m}_\mathrm{e} = \boldsymbol{m}_\mathrm{e}^* - \Delta t\Gamma_\mathrm{F}\boldsymbol{m}_\mathrm{e}\\ &\Leftrightarrow\ \boldsymbol{m}_\mathrm{e} = [1 + \Delta t\,\Gamma_\mathrm{F}]^{-1}\,\boldsymbol{m}_\mathrm{e}^* = \nu\boldsymbol{m}_\mathrm{e}^*.\end{aligned} \tag{31}$$

Again, this yields the implicit equation for the scalar ν to be solved

$$1 - [1 + \Delta t\Gamma_\mathrm{F}]\,\nu = 0. \tag{32}$$

Finally, Eq. (31) yields the updated $\boldsymbol{m}_\mathrm{e}$ and $\lambda_\mathrm{e} = |\boldsymbol{m}_\mathrm{e}|$. Applying this procedure to all N families of fibers delivers a single value ν_i, for each fiber family, respectively.

Remark 2 *Eq.* (6) *could be integrated directly to obtain* J_e *at* t_{n+1} *and update* $\mathbf{b}_\mathrm{e} = J_\mathrm{e}^{2/3}\bar{\mathbf{b}} = J_\mathrm{e}^{2/3}J^{-2/3}\mathbf{b}$. *With predictor* $J_\mathrm{e}^* = (\det\mathbf{h})J_\mathrm{e}^n$ *and corrector* $J_\mathrm{e} = \kappa' J_\mathrm{e}^*$ *one would have to solve instead of* (29)

$$1 - \left[1 + \frac{\Delta t}{\kappa' J_\mathrm{e}^*}\Gamma_\mathrm{M}\right]\kappa' = 0, \tag{33}$$

which generally leads to another result for J_e. *The same update would be obtained only if* $\kappa' = \kappa^{3/2}$. *Inserting this into* (33), *one obtains*

$$1 - \left[1 + \frac{\Delta t}{\kappa^{3/2}J_\mathrm{e}^*}\Gamma_\mathrm{M}\right]\kappa^{3/2} = 0,$$

which differs from (29) *by a factor of* 2/3. *However, with the abbreviation* $z = (\kappa^{3/2} J_{\mathrm{e}}^{*})^{-1} \Delta t \Gamma_{\mathrm{M}}$, *Eqns.* (29) *and* (33) *can be expanded in a Taylor series as*

$$\kappa = (1 + \frac{2}{3} z)^{-1} = 1 - \frac{2}{3} z + O(z^2),$$
$$\kappa = (1 + z)^{-2/3} = 1 - \frac{2}{3} z + O(z^2),$$

respectively, converging to the same result for $z \ll 1$.

Remark 3 *The implicit Euler method may be replaced by other algorithms but care has to be taken that they satisfy the concept of objective integrators [see e.g. Rubin and Papes, 2011; Hollenstein et al, 2013]. For the present calculations, which were free of superimposed rigid body motions by definition, an efficient trapezoidal rule was applied, so that the update* $y = y^{n+1}$ *in Eqns.* (26) *and* (30) *was of the form* $y = y^{*} - (\Delta t/2)(\dot{y}^{n} + \dot{y})$ *instead of* $y = y^{*} - \Delta t\, \dot{y}$.

2.7 Parameter identification

All parameters were obtained by minimizing the weighted least-squares error between model and experimental mean nominal tension and kinematic (contraction) responses from the relaxation phase of uniaxial relaxation tests (R-U). To this end, the model Cauchy stress $\boldsymbol{\sigma}$ (21) was converted to nominal membrane tension $\mathbf{T} = HJ\boldsymbol{\sigma}\mathbf{F}^{-\mathrm{T}}$, where H denotes the thickness of the amnion samples in the reference state. This is treated as an unknown and lumped with μ_0 into a single parameter $\bar{\mu}_0 = H\mu_0$, which has units of force per unit length [cf. Bürzle and Mazza, 2013]. In accordance with this, the parameters $\bar{k}_{\mathrm{M}} = k_{\mathrm{M}}/H$ and $\bar{k}_{\mathrm{F}} = k_{\mathrm{F}}/H$ were defined so that the dissipative rates (22) and, correspondingly, the evolution equations (2) become independent of the membrane thickness H. Finally, the principal tension responses T_j, $j = 1, 2, 3$, were computed for the special cases of uniaxial, strip-biaxial and equibiaxial tension in order to compare with the experimental data. To this end, the experimental local stretch or tension histories in loading direction were used as input and the boundary value problems with corresponding boundary conditions were solved numerically, including the integration of the evolution equations (see Sec. 2.6). This provided at each time point those principal stretches and tensions which were not prescribed, and which were compared to the available experimental responses.

The experimental curves were based on the measured force per initial width of the samples, the optically determined in-plane stretch in loading direction λ_1, the lateral stretch λ_2 (both evaluated in the central area of the specimen) and the thickness ratio λ_3 of the membrane acquired by multiphoton microscopy, see [Mauri et al, 2015c,b] for details. Experimental data were obtained from mechanical tests performed on term fetal membranes. Mean curves of the relaxation uniaxial experiments, used for parameter identification, were computed as explained in the Appendix. We emphasize that the reconstructed loading was not included in the objective function for parameter identification.

The initial values of the parameters $\bar{\mu}_0$, q, $m_{2,4,5}$, $\bar{m}_3$ and ϑ followed from the values that had been identified for the compressible elastic model described in Sec. 2.5. For the remaining parameters $\bar{k}_{\mathrm{M,F}}$ and α_{M}, which control the dissipative behavior in the matrix and fibers, starting values were chosen such that both the relaxation and creep response were qualitatively captured. Minimization of the objective function was performed based on the MATLAB routine fminsearch. The parameter set obtained by this means is given in Table 1.

Table 1 Parameters representing the fitting to the mean relaxation curve under uniaxial tension configuration.

	R-U
General parameters	
$\bar{\mu}_0$ [N/mm]	$2.2153\ 10^{-3}$
q [-]	2.9215
Matrix parameters	
m_1 [-]	$1.3677\ 10^{+1}$
m_2 [-]	$9.2900\ 10^{-5}$
m_5 [-]	3.0456
$\bar{k}_{\mathrm{M}}$ [mm/Ns]	$6.7596\ 10^{+1}$
α_{M} [-]	5.655
Fiber parameters	
$\bar{m}_3$ [-]	$3.1863\ 10^{+1}$
m_4 [-]	$6.7908\ 10^{-1}$
ϑ [°]	$1.0907\ 10^{+1}$
$\bar{k}_{\mathrm{F}}$ [mm/Ns]	$1.0166\ 10^{-4}$

After identifying the parameters by adjustment of the model to the mean relaxation curve, the model was compared to each individual experiment in a second step, where all parameters except the factor $\bar{\mu}_0$ were kept constant. The specimen specific $\bar{\mu}_0$ was determined by comparing one single value from experiment and simulation. In the uniaxial and strip-biaxial relaxation tests, this value was the peak tension at the end of the (sample specific) loading ramp. For uniaxial creep tests, the value of λ_1 at the beginning of the creep phase was used. The so-obtained agreement between experiments and simulations is illustrated in the next section.

3 Results

3.1 Mean relaxation response

The fitted volumetric time-dependent model is shown in Fig. 2 and compared with the mean experimental data from Mauri et al [2015c]. The proposed model formulation nicely captures the large tension relaxation characteristic of the amnion and its corresponding volume changes. The in-plane contraction is slightly underestimated in the initial relaxation phase; however this difference lies within the standard deviation of the experimental results (gray shadow). The out-of-plane stretch λ_3 slightly increases in the first 0.5 s of the very fast loading and finally reaches the long-term value experimentally observed in Mauri et al [2015c].

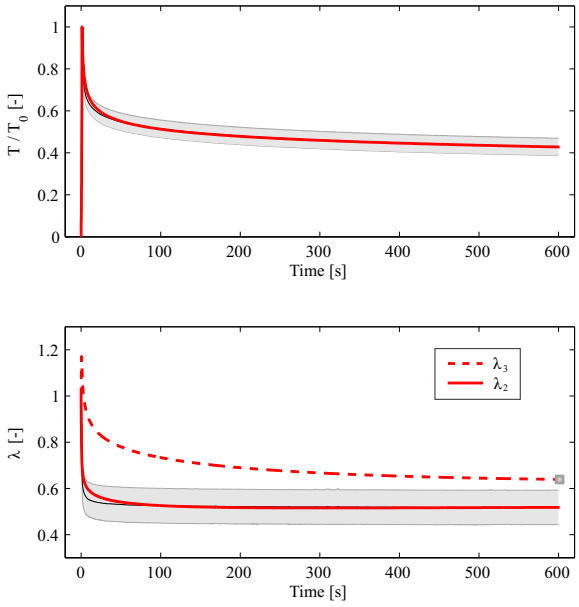

Fig. 2 Fit of the model to the mean relaxation response of the amnion under uniaxial tension configuration (R-U). The experimental mean and standard deviation are shown in gray, and the model in red. The model is able to nicely represent the tension relaxation of the amnion and its in-plane (solid line) and out-of plane (dashed line) kinematic behavior.

3.2 Sample-specific relaxation curves

The model response after adjustment of the parameter $\bar{\mu}_0$ is shown for each experimental curves in Fig. 3. Specimens with a behavior in the variability spread are very well captured with the fit of this single parameter. Note that the logarithmic scale enhances the differences between model and experiment in the loading phase of the relaxation tests, and that few experimental data points were available for the very fast loading phase (less than 2 s) as a result of limitations in the rate of image acquisition. Thus, the differences between model and experiments in the loading regime are due to the fact that the loading phase has not been considered during the parameter identification of the model.

3.3 Prediction of uniaxial creep and strip-biaxial relaxation experiments

This model calibrated with the uniaxial relaxation (R-U) experiments is able to reproduce the very small creep accumulation typical of soft tissues and reported for the human amnion in Mauri et al [2015c]. The variability of the specimens in the uniaxial creep experiments (C-U) could likewise successfully be accounted for by adjustment of the parameter $\bar{\mu}_0$. We restrict in Fig. 4 to presenting the best and worst fitting obtained, to demonstrate the robustness of this procedure. In both cases, the model is able to capture the very small creep strain accumulation in the loading direction and the corresponding creep accumulation in the transverse direction - in addition to the strong lateral contraction during loading. The largest discrepancy between the model and the experimental data occurs in the first part of the fast loading, similarly as for the relaxation experiments.

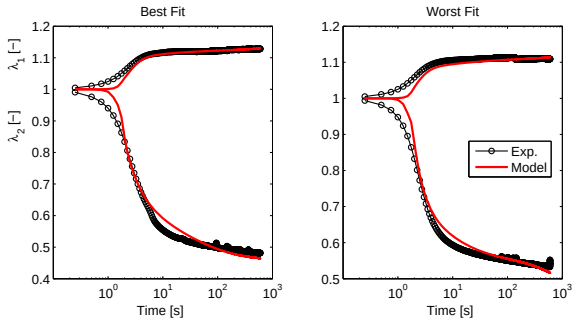

Fig. 4 The in-plane stretches under uniaxial creep configuration (C-U) are shown for the best and worst model fit. The reported curves include the initial loading up to the constant creep force.

The relaxation response of this model formulation under strip-biaxial configuration (R-B) was also computed and compared with the experimental data. In R-B specimens, the biaxial state of tension was obtained by restraining the lateral (but not thickness) contraction during uniaxial extension by a large width-to-length ratio [see e.g. Holzapfel, 2000]. Note that the

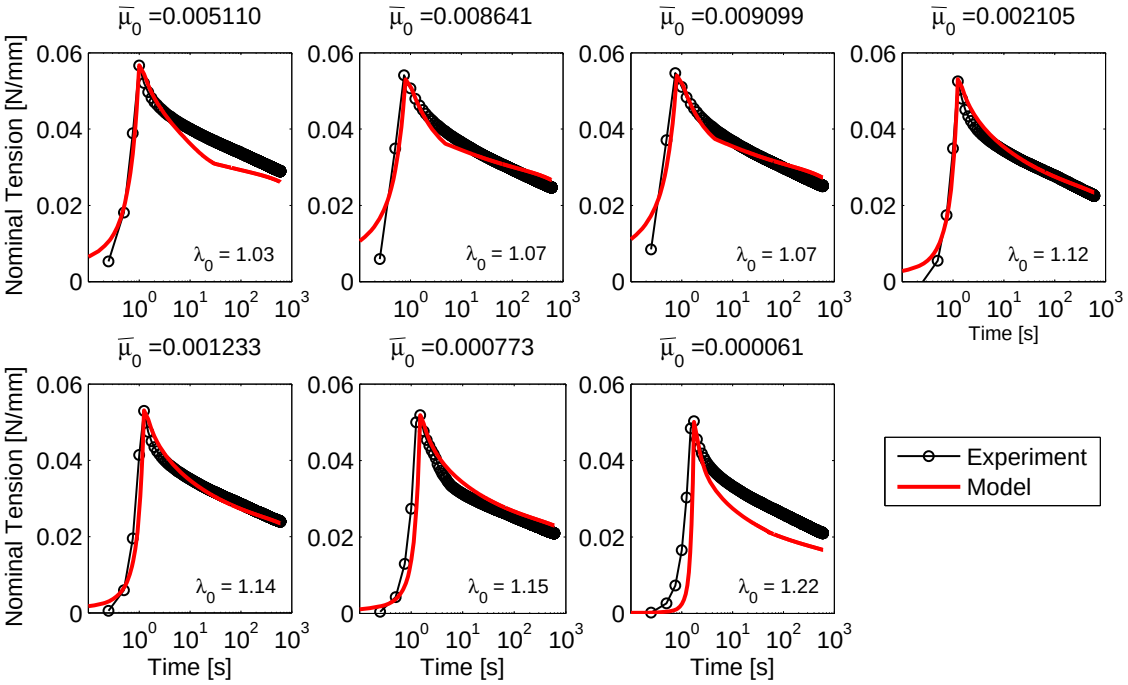

Fig. 3 The value of the $\bar{\mu}_0$ parameter is shown for each R-U specimen. The agreement between experiments and model fitting is remarkable, especially considering that the local stretch during relaxation (λ_0) varies largely among specimens (from 1.07 to 1.22).

relaxation behavior in R-B tests is considerably different from the R-U case [Mauri et al, 2015c]. In particular, the tension level after 10 min drops to 53% of the initial value for strip-biaxial and to 46% for the uniaxial configurations. Similarly as for the C-U data, the best and worst fit are reported in Fig. 5. Although, the model seems to overestimate slightly the nominal tension in the long-term regime, the overall fit is very good for a model calibrated with only uniaxial relaxation data.

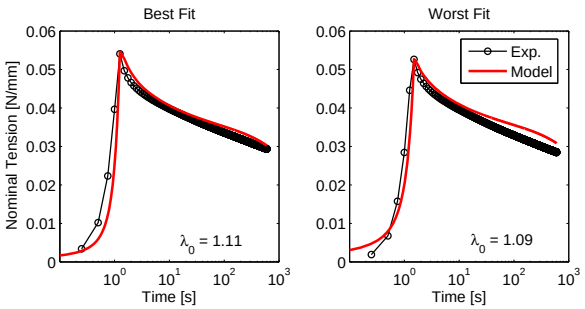

Fig. 5 The best and worst fits are shown for the tension relaxation under strip-biaxial configuration (R-B).

The specimen-specific parameter ($\bar{\mu}_0$) is reported in Table 2 for all considered experiments, showing a variability in the same order of magnitude of the experimental-curves. Notably, its value is also visibly affected by the origin of the membrane, see e.g. M1 and M2, indicating that the distribution of the parameter ($\bar{\mu}_0$) includes both the inter- and intra-subject variability of the healthy human amnion.

Table 2 Specimen-specific parameter $\bar{\mu}_0$ for all membranes.

Specimen	Membrane	$\bar{\mu}_0$ [N/mm]
S1	M1	0.0051099
S2	M1	0.0086409
S3	M1	0.0090991
S4	M2	0.0021045
S5	M2	0.0012331
S6	M2	0.0007733
S7	M2	0.0000609
S8	M3	0.0038194
S9	M3	0.0062780
S10	M4	0.0089720
S11	M4	0.0045275
S12	M4	0.0069782
S13	M5	0.0006646
S14	M5	0.0014564
S15	M5	0.0003088
S16	M5	0.0013915

4 Discussion

4.1 Large tension relaxation but very small creep strain accumulation

This volumetric viscoelastic model based on the framework proposed by Rubin and Bodner [2002] was developed to capture the macroscopic and microscopic mechanical behavior of the human amnion as reported in Mauri et al [2015c]. The large volume reduction observed experimentally motivated the compressible formulation of the viscoelastic model. The 11 parameters contained in the model were fitted to the relaxation response under uniaxial tension configuration (cf. Table 1 and Fig. 2) and used to predict the response of the uniaxial creep (Fig. 4) and strip-biaxial relaxation (Fig. 5) experiments. The viscoelastic behavior of human amnion, especially the interrelation of large tension reduction during relaxation and the very small strain accumulation during creep are encompassed in this model. This interrelation is a characteristic of many soft biological tissues [Thornton et al, 2001; Lakes and Vanderby, 1999] and is missing in the quasilinear viscoelastic (QLV) formulation [Thornton et al, 1997; Haslach, 2005; Oyen et al, 2005; Sopakayang and De Vita, 2011; Anssari-Benam et al, 2012].

Although this model remains phenomenological, elastic and dissipative effects can be associated with matrix and fiber components, based on insights gained with detailed experimental investigations. The present formulation is able to capture the two mechanisms suggested in Mauri et al [2015c] for the time-dependent behavior of the amnion, i.e. a short-term relaxation response related to fiber alignment and water outflow from the matrix on the one hand, and a long-term relaxation related to dissipative fiber behavior on the other one. The coupling between the matrix and the fibers is very strong and determines the resulting equilibrium in the model.

This approach allowed the formulation of a simple model able to reproduce the compressible and time-dependent behavior of human amnion under different multiaxial loading conditions in both relaxation and creep states.

4.2 Inter- and intra-subject variability

Large variability between specimens has typically been observed in previous investigations of the human amnion [e.g. Jabareen et al, 2009; Bürzle and Mazza, 2013] and is reflected by the scatter of the specimen-specific parameter ($\bar{\mu}_0$). El Khwad et al [2005] reported a similar inter- and intra-patient variability in the value of FM strength, which is even larger if specimens of the cervical region are considered. This variability is intrinsic in the material inhomogeneity and correlates with the amount of collagen in the tissue [Bürzle et al, 2013]. We believe that the variability in mechanical response is induced by a different amount of mechanically significant material in the specimen, rather than by differences in its internal organization and microstructure. This hypothesis is in agreement with the results of the renormalization procedure proposed in Mauri et al [2015c], where the relative shift of the curves is neutralized by the normalization of the curves at the common peak force and would also explain the very small variability observed in the normalized curves of the relaxation data [Mauri et al, 2015c; Oyen et al, 2004]. Correspondingly, the differences between specimens can be explained in the proposed modeling formulation by one single parameter $\bar{\mu}_0 = H\mu_0$, which is a coefficient of all tension components (cf. Eqns. (21)).

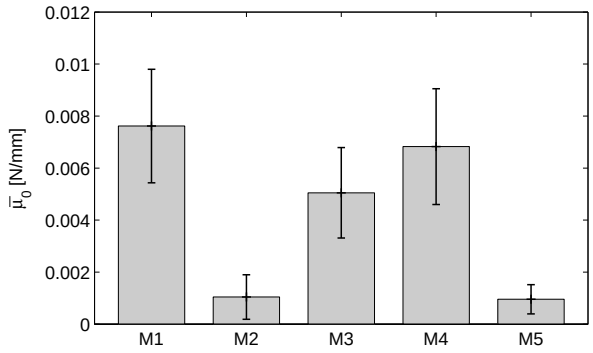

Fig. 6 Distribution of the modeling parameter $\bar{\mu}_0$ within different patients. Parameter values are reported for each membrane (M) as mean ± standard deviation.

As opposed to patient-specific simulations (e.g. Jacobs et al [2014]), where the complete material model is specifically defined for each patient, the presented model can be applied to any FM, with only $\bar{\mu}_0$ as patient specific input. The distribution of $\bar{\mu}_0$ contains the inter- and intra-patient variability (see Fig. 6) and can be used to define a confidence interval representative of the healthy term human amnion. This new interpretation of the model parameter $\bar{\mu}_0$ represents a first step towards a less deterministic and more stochastic view of the material modeling of human tissues. The possibility of including in numerical simulations a prediction range representative of the healthy human tissue, will allow to evaluate the response of amnion in different experimental protocols, under physiological loading conditions (e.g. contractions) or during medical procedures.

4.3 Limitations and future directions

Based on the parameter set reported in Table 1, the equibiaxial creep behavior under constant tension was simulated and compared to the first cycle of the creep inflation experiments in [Mauri et al, 2015c], the results of which were provided in terms of d/d_0, the accumulated apex displacement d of the inflated membrane with respect to the displacement d_0 at the beginning of the creep phase. Adjustment of $\bar{\mu}_0$ and a meaningful quantitative comparison of the model with the test data is only possible by inverse FE analysis. As a first approximation, however, d/d_0 is comparable to the ratio $\varepsilon/\varepsilon_0$, where $\varepsilon = \lambda - 1$ denotes the in-plane strain in the equibiaxially stretched membrane and, again, the subscript 0 refers to its value at the beginning of the creep phase. The result shown in Fig. 7 indicates that

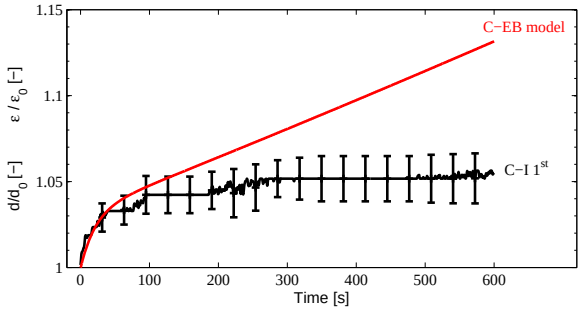

Fig. 7 Prediction of creep in planar equibiaxial tension based on the parameters in Table 1 and comparison with the experimentally observed ratio of apex displacement in creep inflation experiments [Mauri et al, 2015c].

the long-term accumulation of biaxial creep strain is significantly over-predicted by the model. While it is possible to avoid this discrepancy by a more involved formulation of the dissipative rates Γ_{F}^{i} (cf. Eq. (22)), this optimization is beyond the scope of this study, which aimed at the definition of a very simple model formulation able to reproduce the interrelation of uniaxial relaxation and creep behavior.

Generally, a modification of Γ_{M} and Γ_{F}^{i}, which are presently given by simple phenomenological formulations, bears great potential for an improvement of the model. In fact, for Γ_{M} a relation with the theory of porous media (TPM), see e.g. [de Boer, 2000] may be drawn by rewriting (6) such that $J_{\mathrm{e}}\mathrm{tr}\mathbf{d} = \dot{J}_{\mathrm{e}} + \Gamma_{\mathrm{M}}$. This states that the change of current volume of contained water with tissue volume is composed of the change due to the actual (but very small) elastic compressibility, and of Γ_{M}, which can thus be attributed to a dissipative flow of the water through the matrix. According to Darcy's law, the latter should be driven by the pressure gradient in the tissue. Here, due to the membrane dimensions, the latter might be assumed to be dominated by the component in thickness direction [cf. with assumptions in Taber and Puleo, 1996]. Further, the flow may be assumed constant through the thickness, so that the pressure itself becomes the driving force. Indeed, Γ_{M} depends on the hydrostatic pressure term $\mathrm{tr}\boldsymbol{\sigma}_{\mathrm{Me}}$ in the present formulation. Seen from this perspective, the power law down-weighting Γ_{M} with reducing volume in (22) might be motivated with a changing permeability as was realized in refined TPM models [Ehlers and Eipper, 1999].

The constitutive model developed in the present study can be used to investigate the deformation behavior, strength and fracture properties of non-pathological tissue at the end of gestation. Obviously, most clinical questions are related to the mechanical response of amnion earlier in pregnancy or in case of pathological conditions. Future investigations will address preterm tissue and tissues subjected to deterioration associated with biochemical agents [Moore et al, 2006]. The proposed model formulation might be used as a basis to define corresponding constitutive equations to analyze pathological conditions and to identify specific model parameter changes associated with tissue deterioration and preterm rupture. Systematic investigation of the relation between the effect of biochemical factors and mechanical properties will inform corresponding modifications of the model formulation in order to quantify the effect of e.g. inflammatory processes or decidual bleeding [Kumar et al, 2011] on the ability of amnion to resist physiological loading conditions.

5 Conclusion

A compressible and time-dependent model for the human amnion has been formulated and validated. A new approach to the interpretation and definition of its parameters has been presented, which allows representing the intra- and inter-membrane variability with one single parameter. This approach demonstrated the predictive capabilities of the selected formulation for relaxation and creep in uniaxial and biaxial loading states.

Acknowledgements The authors are grateful to the team of Prof. Zimmermann at the University Hospital Zurich for providing FM samples and to the Swiss National Science Foundation (SNSF) for financial support (Project number: 205321 134803/1). AEE gratefully acknowledges the support within the ETH Zurich Postdoctoral Fellowship (FEL13-12-2) and Marie Curie Actions for People COFUND programs. DSADF gratefully acknowledges financial support from the Faculty of Engineering at the University of Nottingham that

enabled a 3-month visiting professorship at the ETH Zurich during the first half of 2013.

Appendix

Experimental materials and methods

The experimental data published in Mauri et al [2015c] were used to calibrate and validate the proposed model. Additional tests were performed to increase the number of R-U specimens from different membranes to better evaluate the model. For these additional amnion samples, after informed written consent of the patients was given (Ethical Committee of the District of Zurich Stv22/2006 and Stv07/07), preparation, testing and post processing were performed as described in Mauri et al [2015c]. All membranes were collected from term elective caesarean sections. The model response under different multiaxial relaxation and creep configurations was computed with the time, force and local strain histories of all experiments. The local in-plane stretches were extracted from the images recorded with 4 Hz through the video extensometer system, similarly to Perrini et al [2015]. The holding stretch in relaxation tests was defined by a target force [cf. Mauri et al, 2015c], which resulted in different values for the stretch due to the variability of the specimen properties. Therefore, the mean relaxation curve was calculated after synchronizing the times for which the target force was reached (times at peak). To simulate the complete deformation history of the experiment, an according representative loading ramp with constant rate was generated from the average local stretch and the average time at the peak.

References

Anssari-Benam A, Gupta HS, Screen HRC (2012) Strain transfer through the aortic valve. Journal of Biomechanical Engineering 134(6):061,003

Ateshian GA, Chahine NO, Basalo IM, Hung CT (2004) The correspondence between equilibrium biphasic and triphasic material properties in mixture models of articular cartilage. Journal of Biomechanics 37(3):391–400

Atkinson TS, Haut RC, Altiero NJ (1997) A poroelastic model that predicts some phenomenological responses of ligaments and tendons. Journal of Biomechanical Engineering 119(4):400–405

Barbarino GG, Jabareen M, Mazza E (2011) Experimental and numerical study on the mechanical behavior of the superficial layers of the face. Skin Research and Technology 17(4):434–444

Beck V, Lewi P, Gucciardo L, Devlieger R (2012) Preterm prelabor rupture of membranes and fetal survival after minimally invasive fetal surgery: A systematic review of the literature. Fetal Diagnosis and Therapy 31(1):1–9

de Boer R (2000) Current State of Porous Media Theory. Springer Berlin Heidelberg

Bourne G (1962) The foetal membranes. Postgraduate Medical Journal 38:193–201

Bürzle W, Mazza E (2013) On the deformation behavior of human amnion. Journal of Biomechanics 46(11):1777–1783

Bürzle W, Haller CM, Jabareen M, Egger J, Mallik AS, Ochsenbein-Kölble N, Ehrbar M, Mazza E (2013) Multiaxial mechanical behavior of human fetal membranes and its relationship to microstructure. Biomechanics and Modeling in Mechanobiology 12:747–762

Coleman BD, Gurtin ME (1967) Thermodynamics with internal state variables. The Journal of Chemical Physics 47(2):597–613

Devlieger R, Millar L, Bryant-Greenwood G, Lewi L, Deprest J (2006) Fetal membrane healing after spontaneous and iatrogenic membrane rupture: A review of current evidence. American Journal of Obstetrics and Gynecology 195(6):1512–1520

Doehring TC, Freed AD, Carew EO, Vesely I (2005) Fractional order viscoelasticity of the aortic valve cusp: An alternative to quasilinear viscoelasticity. Journal of Biomechanical Engineering 127(4):700–708

Ehlers W, Eipper G (1999) Finite elastic deformations in liquid-saturated and empty porous solids. Transport in Porous Media 34(1-3):179–191

Ehlers W, Karajan N, Markert B (2006) A porous media model describing the inhomogeneous behaviour of the human intervertebral disc. Materialwissenschaft und Werkstofftechnik 37(6):546–551

Ehret AE (2011) Generalised concepts for constitutive modelling of soft biological tissues. Dissertation RWTH Aachen University, Lehr-und Forschungsgebiet Kontinuumsmechanik

Ehret AE, Itskov M (2007) A polyconvex hyperelastic model for fiber-reinforced materials in application to soft tissues. Journal of Materials Science 42(21):8853–8863

Ehret AE, Itskov M (2009) Modeling of anisotropic softening phenomena: Application to soft biological tissues. International Journal of Plasticity 25(5):901–919

El Khwad M, Stetzer B, Moore RM, Kumar D, Mercer B, Arikat S, Redline RW, Mansour JM, Moore JJ (2005) Term human fetal membranes have a

weak zone overlying the lower uterine pole and cervix before onset of labor. Biology of Reproduction 72(3):720–726

Flory P (1961) Thermodynamic relations for high elastic materials. Transactions of the Faraday Society 57:829–838

Flynn C, Rubin M (2014) An anisotropic discrete fiber model with dissipation for soft biological tissues. Mechanics of Materials 68:217–227

Fung YC (1993) Biomechanics: Mechanical properties of living tissues. New York: Springer-Verlag

Grashow JS, Sacks MS, Liao J, Yoganathan AP (2006) Planar biaxial creep and stress relaxation of the mitral valve anterior leaflet. Annals of Biomedical Engineering 34(10):1509–1518

Haslach HWJ (2005) Nonlinear viscoelastic, thermodynamically consistent, models for biological soft tissue. Biomechanics and Modeling in Mechanobiology 3(3):172–189

Haupt P (2002) Continuum mechanics and theory of materials, second edition edn. Springer-Verlag Berlin Heidelberg New York

Helfenstein J, Jabareen M, Mazza E, Govindjee S (2010) On non-physical response in models for fiber-reinforced hyperelastic materials. International Journal of Solids and Structures 47(16):2056–2061

Hingorani RV, Provenzano PP, Lakes RS, Escarcega A, Vanderby J Ray (2004) Nonlinear viscoelasticity in rabbit medial collateral ligament. Annals of Biomedical Engineering 32(2):306–312

Hollenstein M, Jabareen M, Rubin M (2013) Modeling a smooth elastic-inelastic transition with a strongly objective numerical integrator needing no iteration. Computational Mechanics 52(3):649–667

Holzapfel GA (1996) On large strain viscoelasticity: Continuum formulation and finite element applications to elastomeric structures. International Journal for Numerical Methods in Engineering 39(22):3903–3926

Holzapfel GA (2000) Nonlinear solid mechanics: a continuum approach for engineering. West Sussex, England: John Wiley & Sons, Ltd

Jabareen M, Mallik AS, Bilic G, Zisch AH, Mazza E (2009) Relation between mechanical properties and microstructure of human fetal membranes: An attempt towards a quantitative analysis. European Journal of Obstetrics & Gynecology and Reproductive Biology 144:S134–S141

Jacobs NT, Cortes DH, Peloquin JM, Vresilovic EJ, Elliott DM (2014) Validation and application of an intervertebral disc finite element model utilizing independently constructed tissue-level constitutive formulations that are nonlinear, anisotropic, and time-dependent. Journal of Biomechanics 47(11):2540–2546

Kumar D, Schatz F, Moore R, Mercer B, Rangaswamy N, Mansour J, Lockwood C, Moore J (2011) The effects of thrombin and cytokines upon the biomechanics and remodeling of isolated amnion membrane, in vitro. Placenta 32(3):206–213

Lakes RS, Vanderby R (1999) Interrelation of creep and relaxation: A modeling approach for ligaments. Journal of Biomechanical Engineering 121(6):612–615

Lavery JP, Miller CE (1977) The viscoelastic nature of chorioamniotic membranes. Obstetrics and Gynecology 50(4):467–472

Limbert G, Middleton J (2004) A transversely isotropic viscohyperelastic material: Application to the modeling of biological soft connective tissues. International Journal of Solids and Structures 41(15):4237–4260

Mauri A, Perrini M, Mateos J, Maake C, Ochsenbein-Kölble N, Zimmermann R, Ehrbar M, Mazza E (2013) Second harmonic generation microscopy of fetal membranes under deformation: Normal and altered morphology. Placenta 34(11):1020–1026

Mauri A, Ehret A, De Focatiis D, Mazza E (2015a) Characterization and modeling of the mechanical behavior of human amnion. In: Proceedings of the 16th International Conference on Deformation, Yield and Fracture of Polymers, Kerkrade, NL

Mauri A, Ehret AE, Perrini M, Maake C, Ochsenbein-Kölble N, Ehrbar M, Oyen ML, Mazza E (2015b) Deformation mechanisms of human amnion: Quantitative studies based on second harmonic generation microscopy. Journal of Biomechanics 48(9):1606–1613

Mauri A, Perrini M, Ehret AE, Focatiis DSD, Mazza E (2015c) Time-dependent mechanical behavior of human amnion: Macroscopic and microscopic characterization. Acta Biomaterialia 11:314–323

Mazza E, Papes O, Rubin M, Bodner S, Binur N (2005) Nonlinear elastic-viscoplastic constitutive equations for aging facial tissues. Biomechanics and Modeling in Mechanobiology 4(2-3):178–189

Mazza E, Nava A, Hahnloser D, Jochum W, Bajka M (2007) The mechanical response of human liver and its relation to histology: An in vivo study. Medical Image Analysis 11(6):663–672

Menon R, Nicolau NN, Bredson S, Polettini J (2015) Fetal membranes: Potential source of preterm birth biomarkers. General Methods in Biomarker Research and their Applications pp 483–529

Moore R, Mansour J, Redline R, Mercer B, Moore J (2006) The physiology of fetal membrane rupture: Insight gained from the determination of physical properties. Placenta 27(11-12):1037–1051

Nguyen T, Jones R, Boyce B (2007) Modeling the anisotropic finite-deformation viscoelastic behavior of soft fiber-reinforced composites. International Journal of Solids and Structures 44(25-26):8366–8389

Oxlund H, Helmig R, Halaburt J, Uldbjerg N (1990) Biomechanical analysis of human chorioamniotic membranes. European Journal of Obstetrics & Gynecology and Reproductive Biology 34(3):247–255

Oyen ML, Calvin SE, Cook RF (2004) Uniaxial stress-relaxation and stress-strain responses of human amnion. Journal of Materials Science: Materials in Medicine 15(5):619–624

Oyen ML, Cook RF, Stylianopoulos T, Barocas VH, Calvin SE, Landers DV (2005) Uniaxial and biaxial mechanical behavior of human amnion. Journal of Materials Research 20(11):2902–2909

Oyen ML, Calvin SE, Landers DV (2006) Premature rupture of the fetal membranes: Is the amnion the major determinant? American Journal of Obstetrics and Gynecology 195(2):510–515

Perrini M, Mauri A, Ehret AE, Ochsenbein-Kölble N, Zimmermann R, Ehrbar M, Mazza E (2015) Mechanical and microstructural investigation of the cyclic behavior of human amnion. Journal of Biomechanical Engineering 137(6):061,010

Pierce DM, Maier F, Weisbecker H, Viertler C, Verbrugghe P, Famaey N, Fourneau I, Herijgers P, Holzapfel GA (2015) Human thoracic and abdominal aortic aneurysmal tissues: Damage experiments, statistical analysis and constitutive modeling. Journal of the Mechanical Behavior of Biomedical Materials 41:92–107

Prévost TP (2006) Biomechanics of the human chorioamnion. Master's thesis, Massachusetts Institute of Technology

Reeps C, Bundschuh RA, Pellise k J, Herz M, van Marwick S, Schwaiger M, Eckstein HH, Nekolla SG, Essler M (2013) Quantitative assessment of glucose metabolism in the vessel wall of abdominal aortic aneurysms: correlation with histology and role of partial volume correction. The International Journal of Cardiovascular Imaging 29(2):505–512

Rubin M (1989) A time integration procedure for plastic deformation in elastic-viscoplastic metals. Zeitschrift für angewandte Mathematik und Physik ZAMP 40(6):846–871

Rubin M (1994a) Plasticity theory formulated in terms of physically based microstructural variables-part i. theory. International Journal of Solids and Structures 31(19):2615–2634

Rubin M (1994b) Plasticity theory formulated in terms of physically based microstructural variables-part ii. examples. International Journal of Solids and Structures 31(19):2635–2652

Rubin M (1996) On the treatment of elastic deformation in finite elastic-viscoplastic theory. International Journal of Plasticity 12(7):951–965

Rubin M, Bodner S (2002) A three-dimensional nonlinear model for dissipative response of soft tissue. International Journal of Solids and Structures 39(19):5081–5099

Rubin M, Papes O (2011) Advantages of formulating evolution equations for elastic-viscoplastic materials in terms of the velocity gradient instead of the spin tensor. Journal of Mechanics of Materials and Structures 6(1):529–543

Safadi M, Rubin M (2014) Modeling rate-independent hysteresis in large deformations of preconditioned soft tissues. International Journal of Solids and Structures 51(18):3265–3272

Schriefl AJ, Schmidt T, Balzani D, Sommer G, Holzapfel GA (2015) Selective enzymatic removal of elastin and collagen from human abdominal aortas: Uniaxial mechanical response and constitutive modeling. Acta Biomaterialia 17:125–136

Simo J (1992) Algorithms for static and dynamic multiplicative plasticity that preserve the classical return mapping schemes of the infinitesimal theory. Computer Methods in Applied Mechanics and Engineering 99(1):61–112

Simo J, Taylor R (1982) Penalty function formulations for incompressible nonlinear elastostatics. Computer Methods in Applied Mechanics and Engineering 35(1):107–118

Simo JC, Hughes TJ (2000) Computational Inelasticity, Interdisciplinary applied mathematics, vol 7. Springer-Verlag, Berlin

Sopakayang R, De Vita R (2011) A mathematical model for creep, relaxation and strain stiffening in parallel-fibered collagenous tissues. Medical Engineering & Physics 33(9):1056–1063

Taber LA, Puleo AM (1996) Poroelastic plate and shell theories. In: Selvadurai A (ed) Mechanics of Poroelastic Media, Solid Mechanics and Its Applications, vol 35, Springer Netherlands, pp 323–337

Thornton GM, Oliynyk A, Frank CB, Shrive NG (1997) Ligament creep cannot be predicted from stress relaxation at low stress: A biomechanical study of the rabbit medial collateral ligament. Journal of Orthopedic Research 15(5):652–656

Thornton GM, Frank CB, Shrive NG (2001) Ligament creep behavior can be predicted from stress relaxation by incorporating fiber recruitment. Journal of Rheology (1978-present) 45(2):493–507

Weickenmeier J, Jabareen M (2014) Elastic-viscoplastic modeling of soft biological tissues using a mixed fi-

nite element formulation based on the relative deformation gradient. International Journal for Numerical Methods in Biomedical Engineering 30(11):1238–1262

Yarpuzlu B, Ayyildiz M, Tok OE, Aktas RG, Basdogan C (2014) Correlation between the mechanical and histological properties of liver tissue. Journal of the Mechanical Behavior of Biomedical Materials 29:403–416